The Influence of Internal Charge Transfer on Nonradiative Decay in Substituted Terthiophenes

Adam S. Huss, Ted Pappenfus, Jon Bohnsack, Michael Burand, Kent R. Mann, and David A. Blank*

Department of Chemistry, University of Minnesota, 207 Pleasant Street Southeast, Minneapolis, Minnesota 55455

Received: June 3, 2009; Revised Manuscript Received: August 4, 2009

Photophysical data for a series of end substitued 3′,4′-dibutyl-2,2′:5′,2″-terthiophenes are reported. Static absorption and fluorescence, quantum yields, time-resolved fluorescence, and time- and frequency-resolved pump−probe spectra are applied to investigate excited state relaxation in bromo, nitro, and tricyanovinyl substituted species in a variety of solvents. The effect of solvent polarizability and end-group substitution is discussed in the context of charge transfer in the excited state and its impact on nonradiative decay rates. In solution at room temperature, both symmetric and asymmetric addition of electron withdrawing end groups generate an excited state with substantial charge transfer character. Solvent polarizability has a significant influence on the excited state dynamics in the charge transfer compounds. Examples include a 20-fold reduction in the intersystem crossing rate going from hexane to toluene and an order of magnitude increase in the internal conversion rate between toluene and acetone. The results demonstrate that the impact of the substituents on intramolecular charge transfer, and the resulting amplification of the interactions between the excited state(s) and the local molecular environment, can dramatically change the excited state relaxation dynamics in substituted terthiophenes.

Introduction

Because of their versatility, oligothiophenes have demonstrated significant potential in the fields of organic electronics and photovoltaics.[1−3] One can control the chain length,[4−7] electronically tune the molecules via the addition of electron donating or withdrawing groups,[8−10] and incorporate these molecules into molecular assemblies designed to facilitate excited state charge separation and subsequent transport. In thin films, the addition of electron withdrawing substituents can lead to materials that exhibit both n- and p-type charge transport.[11] In dye-sensitized solar cell architectures, oligothiophenes can be used as a sensitizer, an organic hole conductor, and a linker.[12−19] In organic heterojunction cells, Baeuerle and coworkers have used electron withdrawing dicyanovinyl substituents to improve performance by tuning both the band gap and the open circuit voltage.[20−23] While much of the substitutional tuning focuses on the redox potentials and HOMO/LUMO gaps, the influence of excited state charge transfer on excited state dynamics, such as changes in internal conversion (IC) and intersystem crossing (ISC) rates, can be substantial.

Substitution effects in small chain oligothiophenes have been reported for a variety of substituents. End substitution by bromo, nitro, and methoxy groups has been shown to have a large effect on redox potentials, quantum yields, fluorescence lifetimes, and Stokes shifts in bithiophene and terthiophene.[8] Styrl substitution in the 3′ position of terthiophene, capping the styrl group with a variety of electron donating groups, has been shown to increase both charge transfer character and ISC rates.[24] Cyano substitution has been shown to stabilize both the HOMO and LUMO energy levels.[9] Controlling where on the molecule the substituent is placed allows for fine-tuning of electronic properties. Casado et al. have investigated the influence of both symmetric and asymmetric substitution with nitro and tricyanovinyl (TCV) groups on energetic, electrochemical, and spectroscopic properties.[25] Among their findings, they report a large nonlinear optical (NLO) response for asymmetric TCV substitution, as expected in the case of a charge transfer excited state, and an unexpectedly large NLO response for symmetric TCV substitution.

In this study we use a combination of ultrafast and time integrated spectroscopies to study the influence of electron donor and acceptor substituents on the excited state and dynamics of oligothiophenes. We compare the excited state properties of both symmetric and asymmetric bromine, nitro, and tricyanovinyl substituted 3′,4′-dibutyl-2,2′:5′,2″terthiophene in solution. Stokes shifts, fluorescence quantum yields, and excited state lifetimes are used to quantify the radiative and nonradiative decay rates and estimate the degree of charge transfer in the excited state. Ultrafast time-resolved fluorescence upconversion and pump−probe spectra are employed to unravel the excited state dynamics in a series of solvents with increasing orientational polarizability. The results are considered in terms of the influence of the substitutents on the nature of the excited state, specifically with regard to charge transfer character, and the associated influence on IC and ISC. The results demonstrate that there is not only sensitivity of the excited state dynamics to the nature of the substituent but that the interaction with the polarizable local molecular environment can also exert significant influence.

Experimental Section

Materials. The substituted terthiophenes studied in this project are shown in Figure 1. Synthesis, purification, and electrochemical properties were previously reported.[17,25,26] The unsubstituted 2,2′:5′,2″-terthiophene (Sigma-Aldrich, used as

* To whom correspondence should be addressed. E-mail: blank@umn.edu.

10.1021/jp905218b CCC: $40.75
Published on Web 09/01/2009

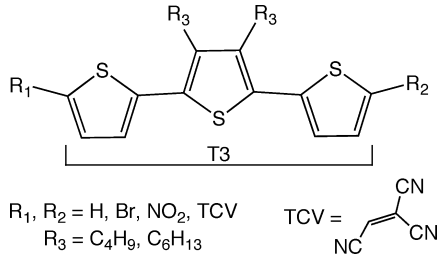

Figure 1. Structures of 3′,4′-dibutyl-2,2′:5′,2″-terthiophene derivatives.

received) was used as a reference for some measurements. All work was done in dilute solution ($\leq 10^{-4}$ M), and no evidence for aggregation was observed in the absorption or fluorescence spectra from any of the samples. Solvents used include pentane, cyclohexane, hexanes, benzene, toluene, xylenes, chloroform, dichloromethane, and acetone. Pentane, cylcohexane, and hexanes were obtained from Fisher Chemicals, benzene from EM Science, and the rest of the solvents were from Mallinckrodt Chemicals. All solvents were ACS grade and were used as received except for benzene and hexanes which were spectrophotometric grade. All experiments in this study were performed at room temperature, which was 296 ± 1 K.

Time Integrated Absorption and Emission. Time integrated absorption and emission spectra were recorded using a Cary 14 running the OLIS globalworks software suite and a Spex Fluorolog 1680 0.2 m double spectrometer running Datamax software, respectively. All spectra were corrected for the detector sensitivity. Quantum yields were measured relative to two standards, either Coumarin 153 in two solvents ($\phi_{fl} = 0.45$ in methanol, 0.84 in cyclohexane)[27] or rhodamine 101 and rhodamine 6G ($\phi_{fl} = 1.0$ and 0.96 in ethanol, respectively).[28,29] Dye samples were purchased from Exciton and used as received. Measuring the dye quantum yields relative to each other gave yields within 10% of the literature values. All emission spectra were measured using 3.10 eV excitation in a 1 cm quartz cell at right angle geometry, except for the tricyanovinyl substituted samples, which were excited at 2.36 eV. Optical densities were less than 0.15, and all solutions were deaerated with argon for 5 min before the spectrum was recorded. On the basis of five measurements successively rotating through rhodamine 101, rhodamine 6G, and 3T-TCV in toluene, we assign a random error for the quantum yield measurements of ±0.002 at the 95% confidence limit. It is likely that the systematics errors are somewhat higher.

Time-Resolved Experiments. ***Time Correlated Single Photon Counting (TCSPC).*** Fluorescence lifetimes longer than 500 ps were measured using TCSPC. The experimental setup has been reported previously.[30] Briefly, deaerated samples in a 1 cm quartz cell were excited using a 40 MHz diode laser (Picoquant LDH-P-C-375) at 3.32 eV. Sample emission was detected using an avalanche photodiode at a right angle geometry at the exit of a double monochromator (Jobin-Yvon TRIAX-320). The instrument response of the system, measured via laser scatter, is approximately 130 ps fwhm.

All other measurements were taken using a home-built, amplified ultrafast Ti:sapphire laser system, which has been described previously.[30] Briefly, a 200 mW, 85 MHz pulse train is produced by a mode-locked oscillator pumped by 2.7 W from a CW Nd:YVO_4 laser (Spectra Physics, Millenia Pro). Selected pulses are amplified at 1 kHz by a home-built regenerative amplifier pumped with a Q-switched Nd:YAG laser (Spectra Physics, Empower 15). After compression, the 810 nm pulses have an energy of approximately 400 μJ and are ~60 fs fwhm assuming a Gaussian profile. Excitation pulses are created by either frequency doubling of the laser fundamental using a 1 mm BBO crystal to create 405 nm pulses or by sending the 810 nm pulses into a home-built two-stage noncollinear optical parametric amplifier (NOPA).[31] The output of the NOPA is tunable between 450 and 700 nm and is typically 60 fs fwhm.

Fluorescence Upconversion. Fluorescence decays shorter than 500 ps were measured using fluorescence upconversion.[32,30] Sample solutions were flowed at 0.25 mL/s through a 1 mm quartz cell from a reservoir kept under argon. The excitation beam was focused to a spot size of 300−400 μm by a 15 cm lens. Sample emission was collected by an elliptical reflector (Melles Griot 02 REM 001) and focused onto a 0.5 mm thick BBO crystal cut for SFG between 450 and 750 nm. The emission was gated with a residual 810 nm pulse, which was focused onto the BBO crystal using a 40 cm lens and overlapped with the sample emission. The timing between the gate and excitation pulses was controlled using the translation of a mirror via a computer controlled delay stage with submicrometer resolution (Newport UMT150PP.1). The upconverted signal was recollimated by a 10 cm focal length lens, dispersed through a fused-silica prism and isolated spatially using a slit positioned between the prism and the input of a monochromator. The signal was then focused onto the entrance slit of a single grating UV monochromator (McPherson 218) by a 30 cm lens and was detected using a photomultiplier tube (Hamamatsu R36-10). The output of the tube was monitored via lock-in detection (Stanford Research 810 Lock-in Amplifier) synchronized to the repetition rate of the laser (1 kHz). The instrument response of this system was approximately 160 fs, measured as the sum frequency of the gate and excitation pulses. The polarization of the excitation pulse was set to the magic angle (54.7°) relative to the gate to remove anisotropic components from the emission decays. Typical excitation energies were 50−80 nJ/pulse, and the observed dynamics showed no dependence on intensity using energies up to 180 nJ/pulse.

Frequency-Resolved Pump−Probe. The pump−probe experiments used the same excitation pulses as described above. The residual 810 nm pulse was focused, via a 15 cm lens, into a 3 mm thick piece of sapphire in order to create a white light continuum probe (spanning 1.24−2.75 eV). The probe continuum was collimated using a 2 cm focus 90° parabola, and a 5 cm focus 90° parabola was used to focus and cross the continuum and the pump beam. The beam size was 20−40 μm at the sample. Typical pump energies ranged from 50 to 75 nJ/pulse, and the measured signal was found to be linearly dependent on pump energy up to 100 nJ/pulse. Samples were flowed, under argon, through a 1 mm quartz cell. After the sample, the probe continuum was collimated using a 5 cm lens and subsequently refocused into a Princeton instruments 2150 monochromator after passing through a 1 mm cuvette containing an ethanol solution of 0.2 mM 1,1′-diethyl-4,4′ cyanine iodide (Sigma-Aldrich, used as received) used to filter out residual 810 nm light from the laser fundamental. The beam was incident on a 150 g/mm grating blazed at 500 nm and was dispersed onto a 256 pixel silicon diode array (Hamamatsu). A National Instruments PCI-6132 A/D card was used to read the entire array after every laser shot, allowing us to collect the entire probe spectrum on a shot-to-shot basis. The frequency of the pump beam was modulated to 500 Hz using a chopper wheel to give an alternating set of probe spectra with and without the pump present. The change in optical density, ΔOD, was recorded after every shot pair. ΔOD spectra were typically averaged for 90 000 laser shots at each time delay. The polarization of the pump

beam relative to the 810 nm used to the make the probe was set to the magic angle (54.7°) to remove anisotropic effects. The instrument response, measured by crossing the probe continuum with the pump beam in an 80 μm thick type 1 BBO crystal (Super Optronics) cut for SFG in the range 1.65−2.75 eV, was ∼100 fs fwhm and independent of probe wavelength.

For early time delays (<1 ps), the signal was corrected for the chirped continuum probe light using a correction curve generated by crossing the probe with a focused 810 nm pulse in a 1 mm piece of fused silica. This generates a cross phase modulation signal that was collected via lock-in detection using a photodiode (Thor Laboratories DET 210) fitted with a 10 nm bandpass filter. The time delay origin for a given probe frequency is determined by fitting of the cross phase modulation signal.[33] Time offsets were determined at seven wavelengths distributed across the white light probe spectrum. The resulting time offsets were then fit to a quadratic dispersion function, which was used to correct the early time spectra. The full frequency data was supplemented with pump probe transients taken at select probe wavelengths using a photodiode with a bandpass filter. These data were taken with a greater density of time points and were fit to determine rise and decay time scales of pump probe features.

The range of our delay stages allows for pump−probe delay times of up to 900 ps. Single time points were taken at 7 or 11 ns by inclusion of an additional (static) delay in the probe line that was 2.1 or 3.3 m long, respectively. While this allows for the collection of the pump−probe spectrum at relatively long delay times it does entail some realignment and a small change in the focus of the probe continuum at the sample. As a result, making quantitative comparisons between signal intensities at long and short delay times is difficult. Therefore, the shape of the spectrum at delays >1 ns should be considered as more reliable than the relative intensity.

Theoretical Calculations. All calculations were performed at the Hartree−Fock 6-31G(d) level using the Gaussian 03 package.[34] Optimized gas phase ground state structures for all of the molecules were obtained, and molecular orbital surfaces were visualized using Gaussview version 4.[35]

Results and Discussion

Time Integrated Absorption and Emission. Absorption and emission spectra for all of the molecules in four solvents are shown in Figure 2, with the molecular structures shown in Figure 1. Some of the emission spectra show structure indicative of a well-resolved vibrational progression. This vibrational progression is spaced by roughly 0.17 eV (1400 cm^{-1}) and is analogous to that seen in most oligothiophenes and polythiophenes. It has been assigned to a carbon−carbon bond stretch.[25,30,36,37] Symmetric bromine substitution (Br-3T-Br) creates a small bathochromic shift in both the absorption and emission. The general shape of the spectrum remains nearly identical to that of the unsubstituted derivative and shows very little sensitivity to solvent. Electron withdrawing nitro end groups cause a much larger bathochromic shift in the absorbance spectrum as well as loss of the vibrational progression in the emission as the solvent polarity increases. The red shift in the emission spectrum with increasing solvent polarity is amplified in Br-3T-NO_2 when compared with NO_2-3T-NO_2; however, the absorbance spectra show very little difference. TCV substitution leads to the largest shift in the absorption and emission spectrum relative to the unsubstituted 3T. Analogous to the symmetric and antisymmetric nitro substitution, the 3T-TCV and TCV-3T-TCV pair have very similar absorption spectra with only minor sensitivity to solvent

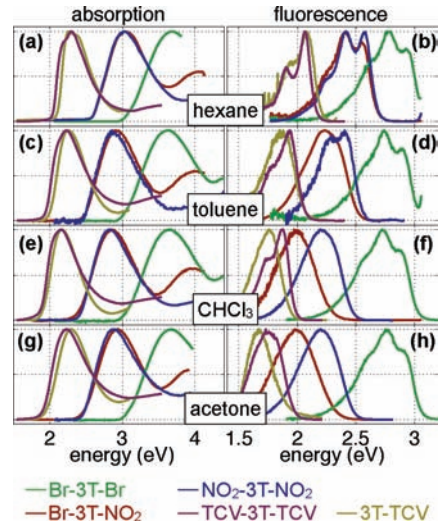

Figure 2. Absorption and emission spectra for the terthiophene derivatives in the indicated solvents.

and a strong solvent dependent bathochromic shift in the emission. In both the nitro and TCV substituted systems, symmetric substitution produces a more pronounced vibrational progression in the emission spectrum.

To quantify the Stokes shifts, the absorption spectra were fit to a single Voigt profile to determine the energy of the maximum, and each emission spectrum was fit to a series of Voigt profiles with a fixed separation to account for the 0.17 eV vibrational progression. The Stokes shift was taken as the difference between the center energy of the absorption Voigt profile and the center energy of the Voigt profile with the highest energy in the emission spectra. This approach was chosen in an effort to maximize consistency of the assignment for comparisons between samples and solvents given the varying amplitudes of vibrational structure in the emission spectra. The absorption maxima, emission maxima, and Stokes shifts are summarized in Tables 1 and 2.

An increase in the Stokes shift with solvent polarity is indicative of a change in the solvent−solute interaction between the ground and excited state of the solute.[38] Assuming the change is dominated by the dipolar interactions, the difference in the magnitude of the dipole moment between the ground and excited state can be estimated from the solvent dependence of the Stokes shift via the Lippert−Mataga relationship:[39−41]

$$\text{Stokes shift} = \frac{2(\Delta\mu)^2}{a^3}\Delta f \qquad (1)$$

In eq 1, $\Delta\mu$ is the difference between the ground and excited state dipole moment magnitudes and a is the Onsager radius, taken here to be 6.2 Å.[24] The orientation polarizability of the solvent is defined as

$$\Delta f = \frac{\varepsilon - 1}{2\varepsilon + 1} - \frac{n^2 - 1}{2n^2 + 1} \qquad (2)$$

In eq 2, ε and n are the solvent dielectric constant and refractive index, respectively. Lippert−Mataga plots are shown in Figure 3 for all of the substituted terthiophenes. Unsubstituted terthiophene is included for reference. Linear least-squares fits to the Stokes shift vs Δf were used to estimate the change in the

TABLE 1: Unsubstituted and Br and NO_2 Substituted Terthiophenes[a]

solvent	Δf	abs_{max} (eV)	em_{max} (eV)	Stokes shift (eV)	ϕ_{fl}	τ_{fl} (ns)	k_r (10^8 s^{-1})	k_{nr} (10^8 s^{-1})	$\Delta\mu^b$ (D)
				3T					
chloroform	0.15	3.73	2.84	0.73	0.050	0.15	3.3	63	
				Br-3T-Br					
hexane	0	3.68	2.77	0.74	0.020	0.042	4.2	230	4
toluene	0.02	3.62	2.74	0.72	0.018	0.049	4.0	200	
chloroform	0.15	3.65	2.78	0.77	0.015	0.036	4.1	270	
acetone	0.28	3.66	2.76	0.75	0.013	0.035	3.8	280	
				NO_2-3T-NO_2					
hexane	0	3.01	2.57	0.43	0.11	0.37	3.0	24	10
toluene	0.02	2.87	2.41	0.46	0.047	0.19	2.5	50	
chloroform	0.15	2.82	2.28	0.54	0.075	0.27	2.8	34	
acetone	0.28	2.87	2.28	0.57	0.082	0.31	2.6	30	
				Br-3T-NO_2					
hexane	0	3.04	2.41	0.48	0.05	0.27	1.9	35	15
cyclohexane	0	3.05	2.45	0.59	0.07	0.31	2.3	31	
benzene	0.005	2.92	2.23	0.60	0.51	2.7	1.9	1.8	
toluene	0.02	2.91	2.24	0.57	0.46	2.5	1.8	2.2	
xylene	0.02	2.91	2.26	0.55	0.42	2.3	1.8	2.5	
chloroform	0.15	2.84	1.99	0.75	0.16	1.3	1.2	6.5	
dichloromethane	0.22	2.84	1.93	0.77	0.13	0.82	1.6	11	
acetone	0.28	2.91	2.00	0.82	0.068	0.49	1.4	19	

[a] Fluorescence spectra and quantum yields were measured exciting at 3.1 eV. Lifetimes shorter than 150 ps were measured exciting near the absorption peak, and longer lifetimes were measured exciting at 3.32 eV. [b] Based on the fit to the Lippert−Mataga plot shown in Figure 3.

TABLE 2: TCV Substituted Terthiophenes[a]

solvent	Δf	abs_{max} (eV)	em_{max} (eV)	Stokes shift (eV)	ϕ_{fl}	τ_{fl} (ns)	k_r (10^8 s^{-1})	k_{nr} (10^8 s^{-1})	$\Delta\mu^b$ (D)
				TCV-3T-TCV					
hexane	0	2.30	2.06	0.24	0.11	0.48	2.3	19	10
toluene	0.02	2.23	1.94	0.30	0.089	0.58	1.5	16	
chloroform	0.15	2.15	1.87	0.28	0.089	0.50	1.8	18	
ethyl acetate	0.20	2.25	1.86	0.38	0.056	0.37	1.5	26	
dichloromethane	0.22	2.15	1.85	0.30	0.061	0.41	1.5	23	
acetone	0.28	2.23	1.75	0.43	0.0079	0.084	0.94	118	
				3T-TCV					
hexane	0	2.27	2.09	0.19	0.029	0.10	2.9	97	15
toluene	0.02	2.26	1.86	0.37	0.039	0.17	2.3	57	
chloroform	0.15	2.17	1.76	0.39	0.0062	0.053	1.2	188	
acetone	0.28	2.29	1.68	0.61	0.0008	0.013[c]	0.61	770	

[a] Fluorescence spectra, quantum yields, and lifetimes for 3T-TCV were measured exciting at 2.25 eV. Spectra and quantum yields were measured for TCV-3T-TCV exciting at 2.43 eV. Fluorescence lifetimes were measured exciting at 3.32 eV. [b] Based on the fit to the Lippert−Mataga plot shown in Figure 3. [c] Determined from the transient absorption at 1.9 eV rather than upconverted fluorescence.

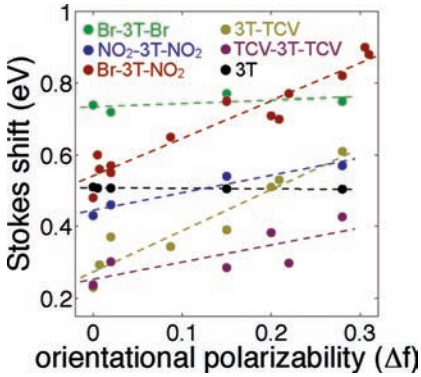

Figure 3. Lippert−Mataga plots for the substituted terthiophenes.

dipole moments, $\Delta\mu$, via eq 1. The resulting values are reported in Tables 1 and 2. It should be noted that the Lippert equation is only an approximation. It does not take into consideration the polarizability of the solute or any change in direction of the dipole moment, and it ignores specific solvent effects like hydrogen bonding or charge-transfer interactions.[38] Modified versions of the Lippert equation have been developed to attempt to account for issues such as the polarizability of the solute.[42−45] However, using these modified approaches did not improve the fits significantly and did not change the trends in $\Delta\mu$, so the original, simplest relationship was employed to obtain the reported values.

The change in dipole moments for the substituted molecules are all much larger than the unsubstituted 3T, which we assume to have a negligible change based on a slightly negative slope in the Lippert−Mataga plot. For the unsubstituted 3T, our data are consistent with a previous report from Clarke et al.[24] Of the substituted molecules, Br-3T-Br had the smallest $\Delta\mu$ value of 4 D, and this increases to 10 D in NO_2-3T-NO_2 and TCV-3T-TCV. The largest $\Delta\mu$ values, 15 D, are found for the asymmetric substitutions in Br-3T-NO_2 and 3T-TCV. A large bathochromic emission shift with solvent polarity is consistent with a large $\Delta\mu$ and suggests an excited state with charge transfer character.[38] Support for charge transfer in Br-3T-NO_2 and 3T-TCV is evident in the molecular orbital surfaces shown in Figure 4. The topologies for the unsubstituted and TCV substituted molecules have been previously reported,[25] and our Hartree−Fock calculations are consistent with those DFT results. On the basis of the

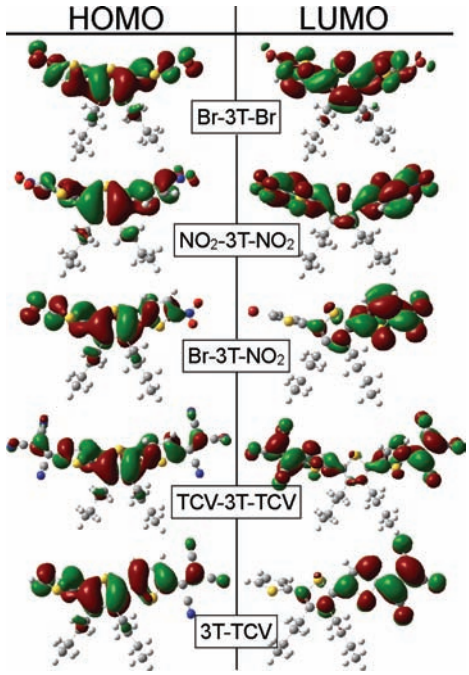

Figure 4. HF 6-31G(d) HOMOs and LUMOs for the terthiophene derivatives. Structures are shown in Figure 1.

molecular orbital diagrams, it was argued that the HOMO → LUMO transition in 3T-TCV is predominately a charge transfer between the terthiophene donor and TCV acceptor. In Figure 4, this type of behavior can be seen in the orbital diagram for both of the asymmetrically substituted molecules, Br-3T-NO_2 and 3T-TCV. The HOMOs are distributed across the terthiophene, while the LUMOs are confined to the end with the electron withdrawing substituent, with very little density remaining on the thiophene ring farthest from the substituent.

Despite the significant $\Delta\mu$ values for the symmetric molecules, there is no evidence of charge transfer character in the orbital diagrams. This is due to the fact that the calculations were done in isolation and therefore cannot account for asymmetries induced by structural reorganization at finite temperatures in a polarizable solvent environment. Casado et al. found that measured hyperpolarizability of TCV-3T-TCV (and TCV-6T-TCV) was significantly higher than predicted by computation, where the symmetric confirmation leads to very little change in the dipole moment and a very small hyperpolarizability.[25] As a possible explanation the authors suggested that the electric field used in the experiments may have broken the symmetry and thereby enhanced the observed NLO response. Our measurements indicate that, at room temperature in solution, the symmetrically substituted molecules have a fair degree of charge transfer in the excited state and a large change in dipole moment. The influence of the polarizable solvent and finite temperature is sufficient to break the symmetry and can explain the unexpectedly large NLO response without the need to implicate the experimental conditions used to measure the hyperpolarizabilities.

Radiative and Nonradiative Decay of the Excited State. Assuming the measured emission is dominated by fluorescence from a single state (the lowest excited singlet state in this case), the radiative and nonradiative decay of that state can be determined from the measured fluorescence quantum yields and lifetimes via eqs 3 and 4.[38]

$$k_r = \frac{\phi_{fl}}{\tau_{fl}} \quad (3)$$

$$k_{nr} = \frac{1 - \phi_{fl}}{\tau_{fl}} \quad (4)$$

In eqs 3 and 4, ϕ_{fl} and τ_{fl} are the fluorescence quantum yield and lifetime, respectively. The measured ϕ_{fl} and τ_{fl} values, along with the resulting values of k_r and k_{nr}, are listed in Tables 1 and 2. On the basis of the error estimates for the quantum yields, we estimate the random errors in the radiative and nonradiative rate coefficients to be roughly 1%. Generally, comparisons show very little sensitivity of the radiative rates to either the substituents or solvents, with the only notable change being the 4-fold decrease in k_r for 3T-TCV as the orientational polarizability of the solvent increases. Nonradiative rate coefficients are at least an order of magnitude larger than the radiative rates in all cases except Br-3T-NO_2, where the nonradiative rate slows for solvents of intermediate polarizability. The nonradiative rates show a sensitivity to both the nature of the substituents and the solvent, with the greatest sensitivity to the solvent apparent in the asymmetric Br-3T-NO_2 and 3T-TCV. These two molecules display an increase in k_{nr} with solvent polarity, gaining an order of magnitude from toluene ($\Delta f = 0.02$) to acetone ($\Delta f = 0.28$). One of the most striking changes is found in Br-3T-NO_2, where k_{nr} decreases by a factor of 20 going from hexane to toluene. This was somewhat unexpected given that this only represents an increase in the dielectric constant of 0.5. After presenting evidence for an associated change in the primary nonradiative decay path, possible origins of this sensitivity are considered in the next section.

In the unsubstituted terthiophene, nonradiative decay has been shown to be much faster than radiative decay.[7,46] Clarke et al. have reported a value of $k_{nr} = 6.8 \times 10^9\ s^{-1}$ for 3T in acetonitrile without alkyl side chains.[24] The fluorescence quantum yield was 0.05, and the fluorescence lifetime was 150 ps. These values are in excellent agreement with our measurements on 3T in chloroform (see Table 1), indicating that the alkyl substitution on the center ring exerts very little influence on the nonradiative decay rates. In small, unsubstituted thiophene oligomers, relatively rapid ISC to a triplet state has been established as being the primary nonradiative decay path.[46−49] In the next section, time-resolved spectroscopy is used to investigate the influence of the substituents and solvents on the rates of, and competition between, ISC and IC.

Time-Resolved Spectroscopy: Excited State Dynamics and the Evidence for Intersystem Crossing. Time- and frequency-resolved pump−probe spectra were collected in a number of solvents, and examples are shown for the terthiophenes in chloroform, hexane, and acetone in Figures 5, 6, and 7, respectively. At short probe delays, the transient spectra have an asymmetric derivative shape resulting from the sum of overlapping positive signals (transient absorption, TA) and negative signals (stimulated emission and ground state bleach). The inverted absorption and emission spectra are shown as dashed lines to indicate the positions, subsequent to spectral diffusion, of any potential stimulated emission and ground state bleach signals.

Unsubstituted Dibutyl-terthiophene, 3T. Figure 5a shows frequency-resolved pump probe spectra for the simplest terthiophene derivative, 3T, in chloroform at a series of pump probe delays. These data are very similar to those previously reported by Rentsch and co-workers[47−50] for terthiophene without alkyl

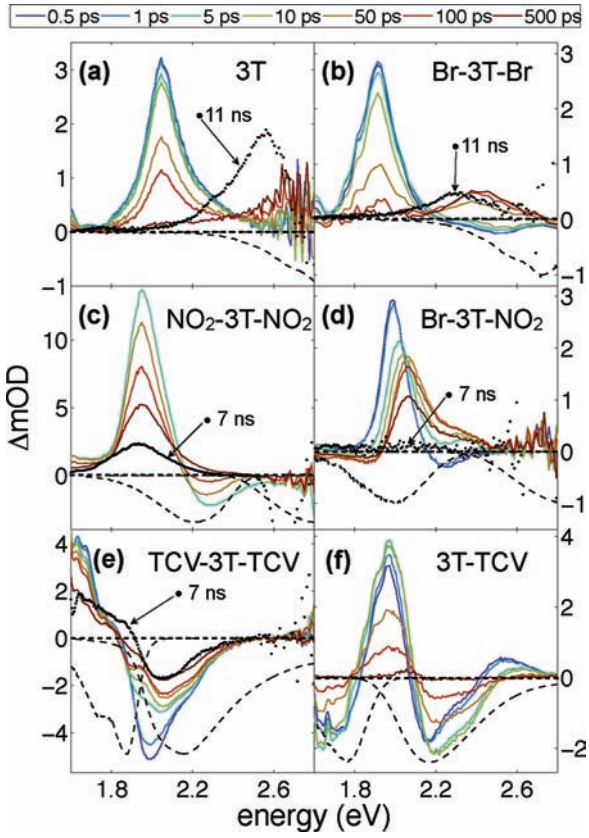

Figure 5. Time-resolved pump−probe spectra for terthiophene derivatives in chloroform excited at 3.1 eV (a−d) or 2.64 eV (e and f). Molecular structures are shown in Figure 1.

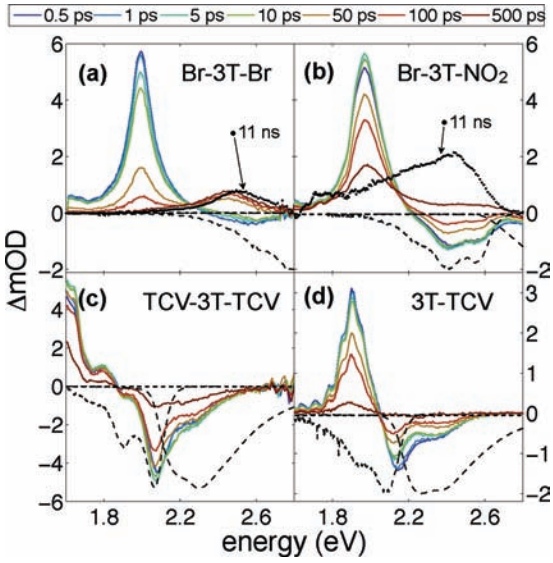

Figure 6. Time-resolved pump−probe spectra for terthiophene derivatives in hexane excited at 3.1 eV. Molecular structures are shown in Figure 1.

substitution. In those studies, the positive feature at 2.1 eV was assigned to an excited singlet state absorption which overlaps partially with the time integrated emission spectrum on the high energy side. In our measurements, this feature appears within the time resolution of the experiment (∼50 fs) and decays on the same time scale as the measured emission, $\tau = 150$ ps. There is some evidence for stimulated emission at early time for energies around 2.5 eV. After the first 500 fs, the spectra in this region are dominated by an increasing TA.

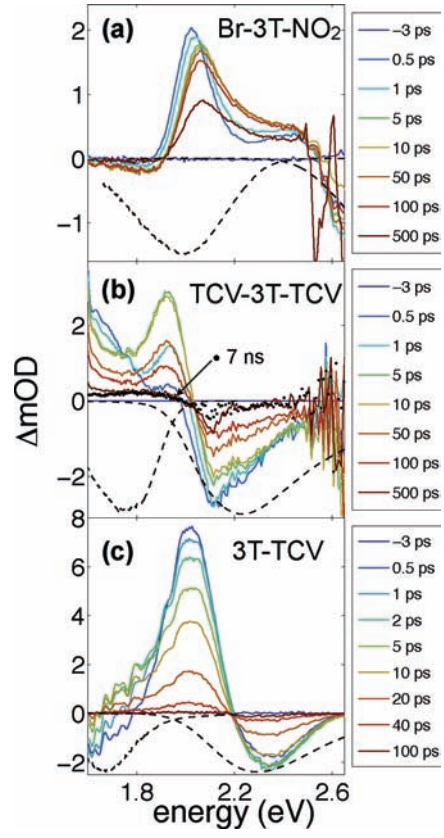

Figure 7. Time-resolved pump−probe spectra for terthiophene derivatives in acetone excited at 3.1 eV (a) or 2.64 eV (b and c). Molecular structures are shown in Figure 1.

The high rate of nonradiative decay from the initially excited singlet state in terthiophene, and most oligothiophenes,[46−49] has been attributed to the heavy atom effect of thiophene sulfur atoms. The enhanced spin−orbit coupling increases the rate of ISC and makes this the primary excited state decay mechanism.[51] In agreement with that prior work, we measure a triplet absorbance around 2.5 eV at long time delays, Figure 5a, which grows in with the same time scale as the decay of the excited singlet absorbance and the fluorescence lifetime. These results confirm that ISC is the primary relaxation mechanism for the unsubstituted dibutyl terthiophene. The solvent dependence of the relaxation rates and pump−probe spectra were not measured for 3T; however, other studies have demonstrated that there is no significant change in the dynamics with solvent for the analogous molecule without alkyl side chains.[24] As will be discussed in detail below, only those molecules that demonstrated excited state charge transfer character show a dramatic solvent dependence of the nonradiative decay rate.

Symmetric Substitution. Pump−probe spectra for Br-3T-Br are shown in chloroform in Figure 5b and in hexane in Figure 6a. The results in the two solvents are nearly identical, and the spectral features are very similar to those in 3T with a small shift to lower energy for both the excited state singlet and triplet absorptions. Compared to 3T, bromine substitution does not influence the radiative decay rate. The short fluorescence lifetime (ca. 50 ps) and associated higher nonradiative decay rate, an increase in k_{nr} of about ×4 over 3T, indicate significant acceleration in the ISC. This is consistent with the well established influence of bromine on the spin−orbit coupling.[52] Analogous results for the nonradiative decay rate following bromine substitution have been shown in similar oligothiophenes and related systems.[8,53] Correlation between the fluorescence

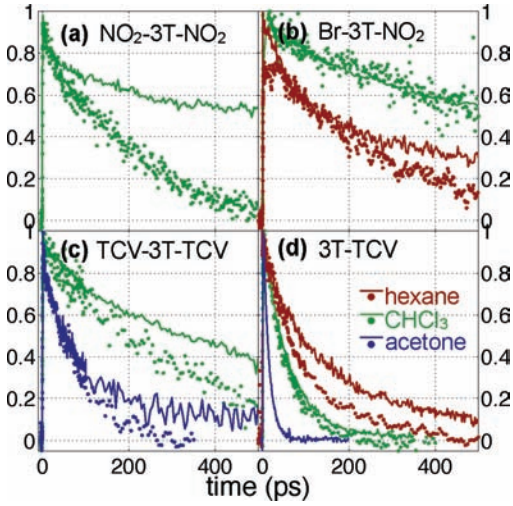

Figure 8. Comparison of pump−probe transients near the maximum of the excited state absorption band (solid lines) with upconverted fluorescence near the maximum of the fluorescence band (solid circles).

lifetime, the decay of the excited state absorption, and the rise in the triplet absorption (Figures 5b and 6a) adds direct evidence to the conclusion that ISC is the primary excited state decay mechanism in both solvents.

The results for symmetric nitro substitution (NO_2-3T-NO_2) are shown in Figure 5c. Compared to 3T, the excited singlet state absorption is shifted to slightly lower energy and appears a bit narrower due to overlapping stimulated emission on the high energy side of the TA. Initially, evidence for a triplet absorption band appears to be absent. However, this is a result of the triplet absorption shifting to nearly the same position (1.9 eV) as the singlet absorption. As shown in Figure 8a, decay in the TA initially follows the fluorescence decay but subsequently diverges after roughly 40 ps. At a time delay of 500 ps, the fluorescence has dropped by >90% and there is no longer clear evidence of stimulated emission from the excited singlet, but the TA feature at 1.9 eV remains strong and persists even at 7 ns; see Figure 5c. Substantial overlap of the TA from the singlet and triplet states complicates the quantitative comparison between the decay of the initially populated excited state and the rise of the triplet absorption. As a result, although there is direct evidence for efficient ISC, it is not possible to rule out a contribution from IC in the measured nonradiative decay rate based on the pump−probe spectra alone. The Lippert−Mataga plot, Figure 3, indicates a fairly significant charge reorganization between the ground and excited states ($\Delta\mu$ = 10 D). Large displacement of the excited state along the collective nuclear reorganization coordinate enhances IC via increasing overlap between ground and excited state wave functions.[24] The lack of increase in the nonradiative decay with the orientational polarizability of the solvent, see Table 1, suggests that IC does not play a competitive role in the excited state relaxation of NO_2-3T-NO_2.

The transient pump−probe signals for TCV-3T-TCV, Figures 5e, 6c, and 7b, are complicated by the red-shifted absorption band that contributes a negative signal (bleach) across much of the probe spectral window. Transient absorption from the excited state appears to overlap both the stimulated emission and ground state bleach. Positive signals are seen where the TA has a larger magnitude than the competing negative signals, on the red side of the stimulated emission, Figures 5e and 6c, and in between the absorption and fluorescence bands, Figure 7b. In all of the solvents except acetone, the excited state dynamics are analogous to NO_2-3T-NO_2. Aside from a slight decline in the radiative rate with solvent polarizability for TCV-3T-TCV, both molecules exhibit only minor changes in the nonradiative rates with solvent, and both have a combined TA and ground state bleach remaining well beyond the emission lifetime at 7 ns ($\tau_{fl} \sim 0.5$ ns). Comparing the fluorescence decay with the decay in the TA signal in Figure 8c, there is a clear divergence in the decay of the two signals after 100 ps with absorbance sustained beyond the decay of the excited singlet state. The remaining absorption, which spectrally overlaps both the excited singlet state absorption and stimulated emission, is assigned to the triplet state and taken as direct evidence of ISC.

Unlike NO_2-3T-NO_2, TCV-3T-TCV shows a 5-fold increase in the nonradiative decay rate and a small decrease in radiative rate in acetone relative to the other solvents. In Figure 7b, the excited state absorption signal around 1.9 eV decays more rapidly than in the other solvents, and while there is a residual absorption at 7 ns, it appears much weaker than the comparable feature in chloroform. As in the case of NO_2-3T-NO_2, the overlapping features in the pump−probe make it difficult to quantify the ISC rate. Comparing the TA and fluorescence decays, see Figure 8c, the decays are more rapid in acetone than chloroform, but in both solvents, the absorption and emission decays track each other for the first 100 ps where they diverge. The fact that the TA and fluorescence signals diverge near the same point in time due to appearance of triplet absorption suggests that the ISC rate is not significantly different in chloroform and acetone. On the basis of this, we conclude that acceleration in the nonradiative decay originates from enhanced IC in acetone. Increase in the IC rate can be explained in terms of additional stabilization of the charge transfer character in the excited state. This type of effect has been previously implicated in comparisons between stryl substituted terthiophenes, where substitution on the stryl group was used to change the degree of charge transfer.[24] In this case, we find that changing the solvent environment can have an analogous influence. Compared with NO_2, the greater electron withdrawing of the TCV substituents, and the associated larger degree of charge separation and structural reorganization in the excited state, enhances this effect. While the Lippert−Mataga plots indicate a similar, large *change* in the solvent−solute interaction with excitation for NO_2-3T-NO_2 and TCV-3T-TCV, the dipole moment in polarizable media at room temperature is likely to be larger for TCV-3T-TCV in both the ground and excited states. The increase in IC rate with solvent polarizability is amplified in the asymmetrically substituted compounds, and this is discussed in the next section.

Asymmetric Substitution. The asymmetrically substituted Br-3T-NO_2 and 3T-TCV show the largest degree of excited state charge transfer, $\Delta\mu$ = 15 D, and the largest sensitivity of the nonradiative decay on solvent orientational polarizability. Figures 5, 6, and 7 present time-resolved pump−probe spectra for both molecules in chloroform, hexane, and acetone, respectively. Both compounds exhibit an initial decrease in k_{nr} going from hexane to toluene, followed by a steady increase in the nonradiative rate with solvent polarizability; see Tables 1 and 2. The initial decrease is much more dramatic in Br-3T-NO_2. With the exception of the rate in hexane, Br-3T-NO_2 has the slowest nonradiative decay rates of the compounds measured, including the analogous symmetric molecules Br-3T-Br and NO_2-3T-NO_2.

We note that the TA feature around 2.0 eV in both chloroform and acetone, Figures 5d and 7a, appears to shift to higher energy

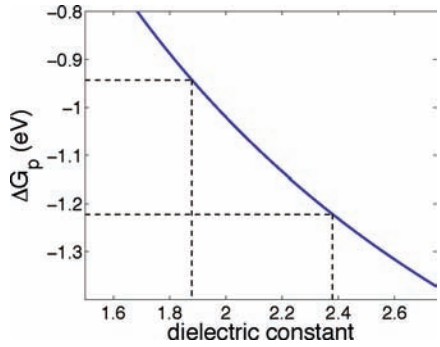

Figure 9. Difference between the solvent polarization energy for a dipole moment of $\mu_1 = 13$ D and $\mu_2 = 18$ D, estimated using the Kirkwood−Onsager expression,[54−57] $\Delta G_p = (\mu_1^2 - \mu_2^2)/a^3[(\varepsilon - 1)/(2\varepsilon + 1)]$. The Onsager radius was set to $a = 6.2$ Å. The dashed lines indicate the values for *n*-hexane ($\varepsilon = 1.88$) and toluene ($\varepsilon = 2.38$).

and broaden during the first 5−10 ps after excitation. Rather than a time dependent shift in the TA itself, we assign this to spectral diffusion of the overlapping negative stimulated emission signals. In Figure 5d, the spectra in the first picosecond after excitation show a negative contribution on the high energy side of the TA. As the delay exceeds 10 ps, this evolves into a positive TA and a new negative feature appears on the low energy side of the TA. This can be explained by spectral diffusion of the stimulated emission signal to lower energy, and we have confirmed that these time scales are exhibited in the emission using fluorescence upconversion. A detailed investigation of the spectral diffusion is left for another study.

Within our signal-to-noise, there does not appear to be any remaining TA at delay times beyond the fluorescence lifetime in solvents other than hexane; for example, see the spectrum at 7 ns in Figure 5d. There is also no detectable divergence between the decay in the TA and upconverted fluorescence signals in the first 500 ps, Figure 8b. This strongly suggests that it is a lack of ISC that is responsible for the reduced k_{nr} values in solvents more polarizable than hexane. In these solvents, the nonradiative rate is primarily dictated by IC, and the rate increases with increasing reorganization and stabilization of the charge transfer excited state. In stark contrast to the other solvents, the results in hexane show clear evidence of ISC. There is a prominent triplet absorption spectrum 11 ns after excitation, Figure 6b, and divergence of decay in the TA and fluorescence ($\tau_{fl} = 270$ ps) beyond 200 ps, Figure 8b.

We ascribe the sudden closure of the ISC channel when going from hexane to toluene (or benzene) to differential solvation of the excited singlet and triplet states shifting ISC from energetically favorable to thermally inaccessible at room temperature. Although there is only a small difference in the dielectric constant between these solvents, $\varepsilon_{hexane} = 1.88$ and $\varepsilon_{toluene} = 2.38$, the very large dipole moment in the charge transfer state provides the potential for large differences in excited state stabilization between the singlet and triplet states. To illustrate this possibility, Figure 9 shows the difference in stabilization energy between a dipole moment of 13 and 18 D as a function of the surrounding dielectric constant (see caption for details). A value of 18 D is chosen as a rough estimate of the excited singlet state based on our measured value of $\Delta\mu$, and 13 D is used to demonstrate how a lower, yet still quite large dipole moment in the triplet state can decrease the stabilization energy. Figure 9 shows that, within the Kirkwood−Onsager continuum model,[55−57] the difference in stabilization increases by nearly 0.3 eV between hexane and toluene. This is sufficient to shift a singlet−triplet pair from near resonance to many multiples of k_BT uphill for ISC at room temperature. Lacking actual knowledge of the triplet dipole moment magnitude, this is offered only as support for the plausibility of our argument. A similar mechanism has been proposed to explain polarity dependent intersystem crossing in twisted donor−acceptor biphenyls.[54] With the substantial decline in the ISC rate, what remains is competition between radiative decay and internal conversion to the ground state.

The nonradiative decay rate for 3T-TCV increases rapidly with solvent polarizability, and in acetone, it exceeds all of the other compounds including the spin−orbit coupling enhanced Br-3T-Br. As in the case of TCV-3T-TCV, the time-resolved pump−probe spectra are complicated by interference from overlapping stimulated emission and the ground state absorption bleach. However, at early time delays, there is a clear TA signal in all solvents between 1.8 and 2.1 eV; see Figures 5f, 6d, and 7c. At a time delay of 500 ps in hexane, well beyond the 100 ps fluorescence lifetime, TA at 1.9 eV remains, and in chloroform, there is also a small, but detectable, TA beyond the lifetime of the excited singlet state. We assign this absorption, which is nearly isoenergetic with the excited singlet absorption, to a triplet state. Figure 8d provides additional evidence for absorption from the triplet state with the divergence between the TA and fluorescence decays in hexane, and to a lesser extent in chloroform.

The modest decrease in k_{nr} between hexane and toluene is suggestive of a mechanism involving reduction of the ISC rate analogous to that seen in Br-3T-NO_2, albeit much less substantial. However, Figure 8d shows that, in hexane and chloroform, with a factor of 2 difference in k_{nr}, decays of the TA and fluorescence signals diverge at very similar points in time. As argued earlier for TCV-3T-TCV, this suggests that there is not a large increase in the ISC rate but rather that the increase in k_{nr} is primarily due to acceleration in the competing IC. This is similar to the results for TCV-3T-TCV, although in that case the acceleration in IC was only observed between the two most polarizable solvents tested. In 3T-TCV, the acceleration in k_{nr} is evident from toluene to acetone, increasing by an order of magnitude and reaching 7.7×10^{10} s^{-1} in acetone. Figures 7c and 8d show that, within our detection limits, there is no measurable TA beyond 80 ps in acetone and no evidence for ISC (note the reduced delay values in the Figure 7c legend). In 3T-TCV, the large degree of charge transfer in the excited state leads to substantial increases in displacement along the collective nuclear reorganization coordinate with increasing solvent polarizability, and the result is a dramatic increase in the IC rate. Evidence for increasing nuclear reorganization with solvent polarizability is also seen in the concomitant decrease of the radiative rate. This is consistent with displacement hindering the radiative transition probability. A similar, although smaller, effect on the radiative rate is seen in Br-3T-NO_2 and TCV-3T-TCV.

Conclusions

We have found that addition of nitro and TCV electron withdrawing substituents to dialkyl terthiophene leads to a charge transfer excited state in the case of both symmetric and asymmetric substitution. Substantial charge separation in the excited state is predicted in the calculated orbital diagrams for the asymmetric molecules. However, the large degree of charge separation observed in the symmetric molecules is not predicted by calculations of the minimum energy state in the gas phase. Finite temperature and the solvent allow a breaking of the symmetry and stabilize the charge separation. Charge transfer

in the excited state and the large associated interaction with the local solvent environment has a significant influence on excited state dynamics, and this can be tuned with the polarizability of the solvent. In Br-3T-NO_2, differential solvation of the excited state changes the primary relaxation path from ISC to IC when going from hexane to toluene, a change of only 0.5 in the dielectric constant. As the polarizability of the solvent increases, the additional stabilization of the charge transfer state increases the displacement of the excited state along the collective nuclear reorganization coordinate, and this accelerates IC. This appears to be a general trend that is amplified with greater charge transfer in the excited state. For 3T-TCV, the IC rate can be tuned by an order of magnitude by choosing solvents with polarizabilities that range between that of toluene and acetone. With work in organic electronics using these types of electron withdrawing substituents to tune the electronic properties of the material, the resulting sensitivity of the excited state dynamics to charge transfer, even in the symmetrically substituted examples, can also have a significant influence on the performance of these materials in applications such as solar cells.

Acknowledgment. This work was funded by a grant from the Chemical Sciences, Geosciences and Biosciences Division, Office of Basic Energy Sciences, Office of Science, U.S. Department of Energy, under Award No. DE-FG02-07ER15913.

References and Notes

(1) Mishra, A.; Ma, C.-Q.; Baeuerle, P. *Chem. Rev.* **2009**, *109*, 1141–1276.
(2) Thompson, B.; Fréchet, J. *Angew. Chem., Int. Ed.* **2008**, *47*, 58–77.
(3) Dimitrakopoulos, C.; Malenfant, P. *Adv. Mater.* **2002**, *14*, 99–117.
(4) Becker, R.; deMelo, J.; Macanita, A.; Elisei, F. *J. Phys. Chem.* **1996**, *100*, 18683–18695.
(5) Grebner, D.; Helbig, M.; Rentsch, S. *J. Phys. Chem.* **1995**, *99*, 16991–16998.
(6) Rentsch, S.; Yang, J.; Paa, W.; Birckner, E.; Schiedt, J.; Weinkauf, R. *Phys. Chem. Chem. Phys.* **1999**, *1*, 1707–1714.
(7) Beljonne, D.; Cornil, J.; Friend, R.; Janssen, R.; Bredas, J. *J. Am. Chem. Soc.* **1996**, *118*, 6453–6461.
(8) Garcia, P.; Pernaut, J.; Hapiot, P.; Wintgens, V.; Valat, P.; Garnier, F.; Delabouglise, D. *J. Phys. Chem.* **1993**, *97*, 513–516.
(9) Demanze, F.; Cornil, J.; Garnier, F.; Horowitz, G.; Valat, P.; Yassar, A.; Lazzaroni, R.; Bredas, J. *J. Phys. Chem. B* **1997**, *101*, 4553–4558.
(10) Hapiot, P.; Demanze, F.; Yassar, A.; Garnier, F. *J. Phys. Chem.* **1996**, *100*, 8397–8401.
(11) Cai, X.; Burand, M. W.; Newman, C. R.; da Silva Filho, D. A.; Pappenfus, T. M.; Bader, M. M.; Bredas, J.-L.; Mann, K. R.; Frisbie, C. D. *J. Phys. Chem. B* **2006**, *110*, 14590–14597.
(12) Chen, R.; Yang, X.; Tian, H.; Sun, L. *J. Photochem. Photobiol., A* **2007**, *189*, 295–300.
(13) Houamer-Rassin, C.; Blart, E.; Buvat, P.; Odobel, F. *J. Photochem. Photobiol., A* **2007**, *186*, 135–142.
(14) Houarner-Rassin, C.; Blart, E.; Buvat, P.; Odobel, F. *Photochem. Photobiol. Sci.* **2008**, *7*, 789–793.
(15) Kim, S.; Choi, H.; Baik, C.; Song, K.; Kang, S. O.; Ko, J. *Tetrahedron* **2007**, *63*, 11436–11443.
(16) Liu, Y.; Nicola, A. D.; Reiff, O.; Ziessel, R.; Schanze, F. *J. Phys. Chem. A* **2003**, *107*, 3476–3485.
(17) Pappenfus, T.; Mann, K. *Inorg. Chem.* **2001**, *40*, 6301–6307.
(18) Thomas, K. R. J.; Hsu, Y.-C.; Lin, J. T.; Lee, K.-M.; Ho, K.-C.; Lai, C.-H.; Cheng, Y.-M.; Chou, P.-T. *Chem. Mater.* **2008**, *20*, 1830–1840.
(19) Wang, Z.-S.; Cui, Y.; Dan-oh, Y.; Kasada, C.; Shinpo, A.; Hara, K. *J. Phys. Chem. C* **2007**, *111*, 7224–7230.
(20) Schueppel, R.; Schmidt, K.; Uhrich, C.; Schulze, K.; Wynands, D.; Bredas, J. L.; Brier, E.; Reinold, E.; Bu, H. B.; Baeuerle, P.; Maennig, B.; Pfeiffer, M.; Leo, K. *Phys. Rev. B* **2008**, *77*, 085311.
(21) Schueppel, R.; Uhrich, C.; Pfeiffer, M.; Leo, K.; Brier, E.; Reinold, E.; Baeuerle, P. *ChemPhysChem* **2007**, *8*, 1497–1503.
(22) Uhrich, C.; Schueppel, R.; Petrich, A.; Pfeiffer, M.; Leo, K.; Brier, E.; Kilickiran, P.; Baeuerle, P. *Adv. Funct. Mater.* **2007**, *17*, 2991–2999.
(23) Scharber, M.; Wuhlbacher, D.; Koppe, M.; Denk, P.; Waldauf, C.; Heeger, A.; Brabec, C. *Adv. Mater.* **2006**, *18*, 789–794.
(24) Clarke, T.; Gordon, K.; Kwok, W.; Phillips, D.; Officer, D. *J. Phys. Chem. A* **2006**, *110*, 7696–7702.
(25) Casado, J.; Delgado, M. C. R.; Merchan, M. C. R.; Hernandez, V.; Navarrete, J. T. L.; Pappenfus, T. M.; Williams, N.; Stegner, W. J.; Johnson, J. C.; Edlund, B. A.; Janzen, D. E.; Mann, K. R.; Orduna, J.; Villacampa, B. *Chem.—Eur. J.* **2006**, *12*, 5458–5470.
(26) Pappenfus, T.; Raff, J.; Hukkanen, E.; Burney, J.; Casado, J.; Drew, S.; Miller, L.; Mann, K. *J. Org. Chem.* **2002**, *67*, 6015–6024.
(27) Lewis, J. E.; Maroncelli, M. *Chem. Phys. Lett.* **1998**, *282*, 197–203.
(28) Fischer, M.; Georges, J. *Chem. Phys. Lett.* **1996**, *260*, 115–118.
(29) Karstens, T.; Kobs, K. *J. Phys. Chem.* **1980**, *84*, 1871–1872.
(30) Wells, N. P.; Boudouris, B. W.; Hillmyer, M. A.; Blank, D. A. *J. Phys. Chem. C* **2007**, *111*, 15404–15414.
(31) Piel, J.; Beutter, M.; Riedle, E. *Opt. Lett.* **2000**, *25*, 180–182.
(32) Kahlow, M.; Jarzeba, W.; DuBruil, T.; Barbara, P. *Rev. Sci. Instrum.* **1988**, *59*, 1098–109.
(33) Kovalenko, S. A.; Dobryakov, A. L.; Ruthmann, J.; Ernsting, N. P. *Phys. Rev. A* **1999**, *59*, 2369–2384.
(34) Frisch, M. J.; Trucks, G. W.; Schlegel, H. B.; Scuseria, G. E.; Robb, M. A.; Cheeseman, J. R.; Montgomery, J. A., Jr.; Vreven, T.; Kudin, K. N.; Burant, J. C.; Millam, J. M.; Iyengar, S. S.; Tomasi, J.; Barone, V.; Mennucci, B.; Cossi, M.; Scalmani, G.; Rega, N.; Petersson, G. A.; Nakatsuji, H.; Hada, M.; Ehara, M.; Toyota, K.; Fukuda, R.; Hasegawa, J.; Ishida, M.; Nakajima, T.; Honda, Y.; Kitao, O.; Nakai, H.; Klene, M.; Li, X.; Knox, J. E.; Hratchian, H. P.; Cross, J. B.; Bakken, V.; Adamo, C.; Jaramillo, J.; Gomperts, R.; Stratmann, R. E.; Yazyev, O.; Austin, A. J.; Cammi, R.; Pomelli, C.; Ochterski, J. W.; Ayala, P. Y.; Morokuma, K.; Voth, G. A.; Salvador, P.; Dannenberg, J. J.; Zakrzewski, V. G.; Dapprich, S.; Daniels, A. D.; Strain, M. C.; Farkas, O.; Malick, D. K.; Rabuck, A. D.; Raghavachari, K.; Foresman, J. B.; Ortiz, J. V.; Cui, Q.; Baboul, A. G.; Clifford, S.; Cioslowski, J.; Stefanov, B. B.; Liu, G.; Liashenko, A.; Piskorz, P.; Komaromi, I.; Martin, R. L.; Fox, D. J.; Keith, T.; Al-Laham, M. A.; Peng, C. Y.; Nanayakkara, A.; Challacombe, M.; Gill, P. M. W.; Johnson, B.; Chen, W.; Wong, M. W.; Gonzalez, C.; Pople, J. A. *Gaussian 03*, revision E.01; Gaussian, Inc.: Wallingford, CT, 2004.
(35) Dennington, R., II; Keith, T.; William, J. *GaussView*, version 4.1; Gaussian, Inc: Shawnee Mission, KS, 2007.
(36) Brown, P.; Thomas, D.; Kohler, A.; Wilson, J.; Kim, J.; Ramsdale, C.; Sirringhaus, H.; Friend, R. *Phys. Rev. B* **2003**, *67*, 064203.
(37) Hennebicq, E.; Pourtois, G.; Scholes, G.; Herz, L.; Russell, D.; Silva, C.; Setayesh, S.; Grimsdale, A.; Mullen, K.; Bredas, J.; Beljonne, D. *J. Am. Chem. Soc.* **2005**, *127*, 4744–4762.
(38) Reichardt, C. *Solvents and Solvent Effects in Organic Chemistry*, 3rd ed.; Wiley-VCH: Weinheim, Germany, 2003.
(39) Lakowicz, J. R. *Principles of Fluorescence Spectroscopy*, 3rd ed.; Springer: Baltimore, MD, 2006.
(40) Lippert, V. E. *Z. Electrochem.* **1957**, *61*, 962–975.
(41) Mataga, N.; Kaifu, Y.; Koizumi, M. *Bull. Chem. Soc. Jpn.* **1956**, *29*, 465–470.
(42) Guo, R.; Kitamura, N.; Tazuke, S. *J. Phys. Chem.* **1990**, *94*, 1404–1408.
(43) Kawski, A. *Z. Naturforsch., A* **2002**, *57*, 255–262.
(44) Sumalekshmy, S.; Gopidas, K. *J. Phys. Chem. B* **2004**, *108*, 3705–3712.
(45) Sumalekshmy, S.; Gopidas, K. *Photochem. Photobiol. Sci.* **2005**, *4*, 539–546.
(46) Rossi, R.; Ciofalo, M.; Carpita, A.; Ponterini, G. *J. Photochem. Photobiol., A* **1993**, *70*, 59–67.
(47) Paa, W.; Yang, J.; Helbig, M.; Hein, J.; Rentsch, S. *Chem. Phys. Lett.* **1998**, *292*, 607–614.
(48) Paa, W.; Yang, J.; Rentsch, S. *Appl. Phys. B* **2000**, *71*, 443–449.
(49) Paa, W.; Yang, J.; Rentsch, S. *Synth. Met.* **2001**, *119*, 525–526.
(50) Lap, D.; Grebner, D.; Rentsch, S. *J. Phys. Chem. A* **1997**, *101*, 107–112.
(51) Rubio, M.; Merchan, M.; Orti, E. *ChemPhysChem* **2005**, *6*, 1357–1368.
(52) Khudyakov, I.; Serebrennikov, Y.; Turro, N. *Chem. Rev.* **1993**, *93*, 537–570.
(53) Mac, M.; Danel, A.; Kizior, K.; Nowak, P.; Karocki, A.; Tokarczyk, B. *Phys. Chem. Chem. Phys.* **2003**, *5*, 988–997.
(54) Maus, M.; Rettig, W.; Bonafoux, D.; Lapouyade, R. *J. Phys. Chem. A* **1999**, *103*, 3388–3401.
(55) Kirkwood, J. G. *J. Chem. Phys.* **1934**, *2*, 351–361.
(56) Onsager, L. *J. Am. Chem. Soc.* **1936**, *58*, 1486–1493.
(57) Cramer, C. J. *Essentials of Computational Chemisty*, 2nd ed.; John Wiley and Sons, Ltd: West Sussex, England, 2004.

JP905218B